HEPATOLOGY

HEPATOBILIARY MALIGNANCIES | HEPATOLOGY, VOL. 74, NO. 5, 2021

Group-2 Innate Lymphoid Cells Promote HCC Progression Through CXCL2-Neutrophil-Induced Immunosuppression

Xingyuan Xu,[1,2*] Longyun Ye,[1,2*] Qi Zhang,[1,2*] Hang Shen,[1,2] Shanshan Li,[1,2] Xiaoyu Zhang,[1,2] Mao Ye,[1,2] and Tingbo Liang [1-3]

BACKGROUND AND AIMS: Due to their inherent characteristics, the function of group-2 innate lymphoid cells (ILC2s) varies in a context-dependent manner. ILC2s are involved in certain liver diseases; however, their involvement in HCC is unknown. In the present study, we assessed the role of an HCC-derived ILC2 population in tumor progression.

APPROACH AND RESULTS: Through FACS and single-cell RNA sequencing, we discovered that ILC2s were highly enriched in human HCC and correlated significantly with tumor recurrence and worse progression-free survival as well as overall survival in patients. Mass cytometry identified a subset of HCC-derived ILC2s that had lost the expression of killer cell lectin-like receptor subfamily G, member 1 (KLRG1). Distinct from their circulating counterparts, these hepatic ILC2s highly expressed CD69 and an array of tissue resident–related genes. Furthermore, reduction of E-cadherin in tumor cells caused the loss of KLRG1 expression in ILC2s, leading to their increased proliferation and subsequent accumulation in HCC sites. The KLRG1$^-$ ILC2 subset showed elevated production of chemotaxis factors, including C-X-C motif chemokine (C-X-C motif) ligand (CXCL)-2 and CXCL8, which in turn recruited neutrophils to form an immunosuppressive microenvironment, leading to tumor progression. Accordingly, restoring KLRG1 in ILC2s, inhibiting CXCL2 in ILC2s, or depleting neutrophils inhibited tumor progression in a murine HCC model.

CONCLUSIONS: We identified HCC-associated ILC2s as an immune regulatory cell type that promotes tumor development, suggesting that targeting these ILC2s might lead to new treatments for HCC. (Hepatology 2021;74:2526-2543).

In the liver, considered as the largest immune organ, resident immune cell populations increase the pathological complexity of HCC, which is a leading cause of cancer-related deaths worldwide.[1] Although tumor-infiltrating lymphoid cells are abundant in HCC tissues,[2] the presence of different subtypes and their divergent interactions with other tumor microenvironment compartments, rendering them incapable of being primed,[3] culminate in tumor progression and even treatment failure. Therefore, identifying the various infiltrating immune cells and determining their interactions within the tumor microenvironment (TME) will lead to improved HCC therapies.

Recently, innate lymphoid cells (ILCs) have been identified in the TME of diverse tumor types.[4] ILCs are a heterogeneous family of innate immune cells lacking rearranged antigen-specific receptors, which are classified into ILC1, ILC2, and ILC3 subsets

Abbreviations: Arg1, arginase 1; BrdU, bromodeoxyuridine; Cdh1, cadherin-1; CFSE, carboxyfluorescein succinimidyl ester; CM, conditioned medium; CXCL, chemokine (C-X-C motif) ligand; GATA3, GATA binding protein 3; GSEA, gene-set enrichment analysis; ICOS, inducible T-cell costimulatory; ILC2, group-2 innate lymphoid cell; KLRG1, killer cell lectin-like receptor subfamily G, member 1; LIN, lineage; n.s., not significant; PBMC, peripheral blood mononuclear cell; PFS, progression-free survival; PTGDR2, prostaglandin D2 receptor 2; PVMC, portal vein blood cell; RNA-seq, RNA sequencing; RPMI-1640, Roswell Park Memorial Institute 1640 medium; scRNA-seq, single-cell RNA-seq; TCR, T-cell receptor; TME, tumor microenvironment; TSLP, thymic stromal lymphopoietin; t-SNE, t-distributed stochastic neighbor embedding.

Received August 20, 2020; accepted March 28, 2021.

Additional Supporting Information may be found at onlinelibrary.wiley.com/doi/10.1002/hep.31855/suppinfo.

[#]These authors contributed equally to this work.

Supported by the National Key Research and Development Project (2019YFC1316000), National Natural Science Foundation of China (81472212 and 81830089 to T.L., 81701630 to L.Y., and 81871320 to Q.Z.), and Zhejiang Science and Technology Bureau's Key Research and Development program (2019C03019).

based on transcription factors, phenotypic markers, and cytokine expression.[5] ILCs are mostly found in the lung, skin, and gastrointestinal mucosa, playing roles in clearing helminth infection, tissue homeostasis, and lymphoid tissue formation.[6] Collectively, IL-33, IL-25, and thymic stromal lymphopoietin (TSLP) are essential for ILC2 activation, because ILC2s lack T-cell receptors (TCRs) or B-cell receptors; however, the important of this is tissue-dependent.[7] Different ILC2 subsets are involved in various inflammatory diseases[8,9] and in liver disorders, such as chronic hepatitis[10] and hepatic fibrosis.[11] Although ILC2s have been investigated in several tumor types, their involvement in HCC is unknown.

Tumor-resident neutrophils can restrict or augment tumor growth, depending on the TME.[12] At the interface between innate and adaptive immunity, neutrophils are recruited by monocytes, macrophages, or epithelial cells through chemokine (C-X-C motif) ligand (CXCL) 5, CXCL2, CXCL1, or monocyte chemoattractant protein-1 to regulate T cells or regulatory T cells.[13] ILC2-expressed Th2 cytokines, such as IL-5 and IL-13, might affect neutrophils functionally in an inflammatory context[10,14]; however, how ILC2s regulate neutrophils in HCC is unclear.

In the present study, we identified a $KLRG1^-$ hepatic ILC2 subpopulation in HCC tissue, which is independent of the ILC2 activators IL-33, IL-25, and TSLP that have been detected in other inflammatory diseases.[9,15] Mediated by low E-cadherin levels, relief of killer cell lectin-like receptor subfamily G, member 1 (KLRG1) signaling induced ILC2 proliferation and CXCL2 and IL-13 production. The latter attracted neutrophils to the tumor site and up-regulated arginase 1 (*Arg1*), which suppressed T-cell activation. Taken together, the hepatic ILC2-CXCL2-neutrophil axis induced an immunosuppressive TME that enabled tumor progression.

Materials and Methods

HUMAN CLINICAL SPECIMENS

The project was approved by the ethics committee of the First Affiliated Hospital and the Second Affiliated Hospital, Zhejiang University School of Medicine. All samples were anonymously coded according to local ethical guidelines. Informed patient consent was obtained.

CELLS

Murine ILC2 cells were isolated from the liver of recombinant IL-33-treated C57BL/6 or CD45.1 mice and were cultured with 10 ng/mL recombinant murine IL-2 (Pepro Tech, Cranbury, NJ) and IL-33 (Pepro Tech) in Roswell Park Memorial Institute 1640 (RPMI-1640) medium. Culture methods for other cell lines are described in the Supporting Information.

MICE

Six-week-old to 8-week-old male C57BL/6JNju were purchased from the Model Animal Research Center of Nanjing University (Nanjing, China), and congenic

View this article online at wileyonlinelibrary.com.
DOI 10.1002/hep.31855

Potential conflict of interest: Nothing to report.

ARTICLE INFORMATION:

From the [1]Department of Hepatobiliary and Pancreatic Surgery, the First Affiliated Hospital, Zhejiang University School of Medicine, Hangzhou, China; [2]Zhejiang Provincial Key Laboratory of Pancreatic Disease, Hangzhou, China; [3]Innovation Center for the Study of Pancreatic Disease of Zhejiang Province, Hangzhou, China.

ADDRESS CORRESPONDENCE AND REPRINT REQUESTS TO:

Tingbo Liang, M.D., Ph.D.
Department of Hepatobiliary and Pancreatic Surgery
the First Affiliated Hospital
Zhejiang University School of Medicine
No. 79 Qingchun Road
Hangzhou 310003, China
E-mail: liangtingbo@zju.edu.cn
Tel.: +86-571-87236601

B6 mice with a CD45.1 allelic marker were obtained from the Jackson Laboratory (Bar Harbor, ME). The mice were bred and housed under pathogen-free conditions at an animal facility. All animal experiments were conducted according to the protocols approved by the Ethics Committee of the First Affiliated Hospital, Zhejiang University School of Medicine.

ESTABLISHMENT OF THE *IN SITU* TUMOR MODEL

The *in situ* HCC model was established as described previously.[16] Detailed procedures are given in the Supporting Information.

ISOLATION OF IMMUNE CELLS FROM DIFFERENT TISSUES

A digestion solution containing 2% fetal bovine serum RPMI-1640, type IV collagenase (1 mg/mL; Worthington, Lakewood, NJ) and DNase (15 μg/mL; Sigma-Aldrich, St. Louis, MO) was used for chemical digestion. Methods of isolation and digestion for different tissues are described in the Supporting information.

FLOW CYTOMETRY AND FACS

Single-cell suspensions were stained with different antibody panels according to specific experimental designs, as described in the manufacturer's instructions. Please refer to the Supporting information for the detailed procedures and antibody list (Supporting Table S1).

MASS CYTOMETRY STAINING AND ANALYSIS

Mass cytometry was performed by PLTTech Inc. (Hangzhou, China). The protocol has been described previously.[17] The antibodies used in the assay are listed in Supporting Table S2. The detailed staining procedures are given in the Supporting Information.

PREPARATION OF THE CONDITIONED MEDIUM

ILC2-PCDH-GFP, ILC2-PCDH-KLRG1, ILC2-CRISPR-GFP, and ILC2-CRISPR-KLRG1 cells (1×10^5) were seeded in 24-well plates and cultured in RPMI-1640 with 10 ng/mL IL-2 and IL-33. The supernatant was collected and filtered after 3 days of culture.

CARBOXYFLUORESCEIN SUCCINIMIDYL ESTER LABELING

According to the manufacturer's instructions, sorted ILC2s or T cells were incubated with 0.5 μM carboxyfluorescein succinimidyl ester (CFSE) labeling (BioLegend, San Diego, CA) in 1 mL of PBS for 15 minutes at 37°C, and quenched using a 5× volume of precooled complete medium. The labeled cells were then used for co-culture experiments.

WESTERN BLOTTING

Total protein from frozen human liver tissues or cell lines was extracted using radio immunoprecipitation assay buffer (Thermo Fisher Scientific, Waltham, MA). Please refer to the Supporting Information for the detailed procedures. The primary antibodies used are listed in Supporting Table S1.

RNA EXTRACTION AND QUANTITATIVE REAL-TIME REVERSE-TRANSCRIPTION PCR

RNA was extracted using Trizol (Thermo Fisher Scientific) and reverse-transcribed to complementary DNA (cDNA), which was subjected to quantitative PCR, and was performed on an Applied Biosystems 7500 Fast Real-Time PCR System (Foster City, CA) according to the manufacturer's instructions. Please see the Supporting Information for the detailed procedures and sequence information (Supporting Table S3).

RNA SEQUENCING AND GENE-EXPRESSION ANALYSIS

RNA sequencing (RNA-seq) was performed using the Illumina Hiseq XTEN platform (San Diego, CA) at Novogene Co. Ltd. (Beijing, China). Gene-set enrichment analysis (GSEA) was performed using the online tool of the LC Bio Cloud Platform (https://www.omicstudio.cn/tool). Morpheus was used for

heatmap visualization (https://software.broadinstitute.org/morpheus/). Please refer to the Supporting Information for the detailed procedures. Raw data were deposited in the GEO database (accession number GSE151895).

SINGLE-CELL RNA-Seq AND ANALYSIS

Single-cell RNA-seq (scRNA-seq) was performed using the Illumina HiSeq PE150 platform at Novogene following standard procedures, as described in the Supporting Information. The t-distributed stochastic neighbor embedding (t-SNE) analysis and cell clustering were performed using the Loupe Cell Browser (version 3.1.0; 10X Genomics, Pleasanton, CA).

IN VIVO BROMODEOXYURIDINE ASSAY

At 4-5 weeks after establishment of the *in situ* HCC model by hydrodynamic injection of oncogene plasmids (when the tumor nodules were macroscopically visible), the mice were injected intraperitoneally with 1 mg of bromodeoxyuridine (BrdU; Becton, Dickinson and Co., Franklin Lakes, NJ). After 24 hours, the hematopoietic cells from their livers were extracted and analyzed for BrdU incorporation using flow cytometry, according to the manufacturer's instructions.

PLASMID CONSTRUCTION, LENTIVIRAL PRODUCTION, AND INFECTION

The mouse cadherin-1 (*Cdh1*) and *Klrg1* cDNAs were cloned into the pCDH-CMV-MCS-EF1a-copGFP lentiviral vector (System Biosciences, Palo Alto, CA) and single-guide RNAs of *Klrg1*, *Cdh1,* and *Cxcl2* were ligated into the lentiCRISPRV2(GFP) vector (Hebio, Shanghai, China), based on previously published protocols.[18] Please refer to Supporting Information Table S3 for the detailed procedures and sequence information.

HEPATIC ILC2 ISOLATION FROM MURINE LIVER

Wild-type mice were injected peritoneally with 400 ng of recombinant murine IL-33 (Thermo Fisher Scientific) every day for 7 days. The mice were sacrificed, and hematopoietic cells from their livers were stained for ILC2s and isolated using FACS. Primary ILC2s were cultured *in vitro* in the presence of 10 ng/mL IL-2 and IL-33.

IN VIVO APPLICATION OF ILC2s

On day 14 after the *in situ* HCC models were established, 1×10^5 of ILC2s, ILC2-PCDH-KLRG1, ILC2-CRISPR-KLRG1, and ILC2-CRISPR-CXCL2 cells, and related control cells were resuspended in 200 μL of PBS and injected through the caudal vein, every 3 days, following the experimental design. The mice were sacrificed after 2-4 weeks of injection.

OTHER TECHNIQUES

Please consult the Supporting Information for the detailed procedures used for the following techniques: magnetic-activated cell sorting, immunohistochemistry, cell proliferation assay of $CD8^+$ T cells, chemoattractant assay, recombinant human E-cadherin binding experiments, *in vitro* co-culture of ILC2 and Hepa1-6 or AML-12 cells, ELISA, immunofluorescence, adoptive infusion of CD45.1-ILC2s, *in vivo* neutrophil depletion assay, and hematoxylin and eosin staining.

STATISTICAL ANALYSIS

Statistical analysis was conducted using GraphPad Prism 6 (GraphPad Inc., San Diego, CA) or SPSS (IBM Corp., Armonk, NY). Please see the Supporting Information for the detailed procedures.

Results

ABUNDANCE OF ILC2s IN TUMOR CORRELATES WITH HCC PROGNOSIS

As previously defined in human tissues, we isolated and defined the $CD45^+$lineage $(LIN)^-CD127^+CRTH2^+$ cells expressing high levels of GATA binding protein 3 (GATA3) from the paired human tumor and nontumoral liver

tissues (n = 150) as ILC2s (Supporting Fig. S1A,B). Taking normal liver tissues without inflammation and fibrosis from excised liver hemangiomas as controls, we found that the percentage of ILC2s (gated as $CD45^+LIN^-CD127^+CRTH2^+$) in the LIN^- subset was substantially elevated in tumors (Fig. 1A). Consistent results were obtained regarding the percentage of ILC2s in the LIN^- subset (Fig. 1B) when the ILC2s were defined as $CD45^+LIN^-CD127^+CRTH2^+GATA3^+ROR\gamma t^{lo}$ (Supporting Fig. S1C) in another cohort of paired HCC and nontumoral tissues (n = 28). The absolute number of ILC2s per gram of tumor tissue of these two patient cohorts were elevated (Supporting Fig. S1D-F). In addition, the percentages of ILC2s in the $CD45^+$ subset and total lymphocytes in the liver, especially in tumors, were higher compared with those in peripheral blood mononuclear cells (PBMCs) or portal vein blood cells (PVMCs) (Fig. 1C, left two panels). The proportions of total ILCs relative to the number of $CD45^+$ cells were also elevated in tumor tissues (Fig. 1C, right panel), which suggested that the ILC2s in the HCC microenvironment were proliferating and accumulating. Similar results were obtained from the second cohort (Fig. 1D). Given the differential frequency of ILC2s between HCC and nontumoral livers, we next investigated whether there was a correlation between ILC2s and patient survival. To minimize the effect caused by patient heterogeneity, we normalized the proportion of ILC2s in the LIN^- population of HCC tissues to that of their respective nontumoral liver controls. The median value was set as the cutoff point to divide the 150 cases of HCC into ILC2 high-abundance or low-abundance groups. Patients with a high tumor/nontumor ILC2 ratio survived worse, with both of their progression-free survival (PFS) and overall survival affected (Fig. 1E). Among various clinical pathological factors (Supporting Table S4), HBV infection, microvascular invasion, and recurrence correlated positively with hepatic ILC2 abundance in patients with HCC (Fig. 1F). Univariate and multivariate analyses showed that tumor-node-metastasis stage and a high tumor/nontumor ILC2 ratio were independent factors for the incidence of recurrence and patient survival (Supporting Tables S5-S7). These data indicate that hepatic ILC2 abundance correlates strongly with HCC progression.

PHENOTYPE OF HEPATIC ILC2s IN THE HCC MICROENVIRONMENT

To identify the human liver tumor–derived ILC2s, we sorted LIN^- hematopoietic cells from one HCC and nontumoral liver tissues, and applied scRNA-seq. As shown in the t-SNE plots, the ILC2 cluster from HCC (18.3%) was enlarged compared with that from the nontumoral tissue (4.2%) when confined to LIN^-CD127^+ cells (Fig. 2A,B), which was consistent with the statistical results from flow cytometry (Fig. 1). The mRNA expression pattern of known ILC2 selective (e.g., *GATA3*, prostaglandin D2 receptor 2 [*PTGDR2*], inducible T-cell costimulatory [*ICOS*], killer cell lectin like receptor B1 [*KLRB1*], *KLRG1*, *IL-2RA*) and exclusive (e.g., T-box transcription factor 21 [*TBX21*], eomesodermin [*EOMES*], RAR related orphan receptor C [*RORC*]) genes validated the identity of these ILC2s under HCC conditions (Fig. 2C). We further confirmed our findings using CNGB Nucleotide Sequence Archive scRNA-seq data (CNP0000650) acquired from 18 patients with HCC (Supporting Fig. S2A,B and Fig. 2D). To verify our finding at the protein level, we used mass cytometry and confirmed a series of ILC2 phenotypic ($ICOS^+CD25^+CD161^+CD117^{+/-}KLRG1^{+/-}$; Fig. 2E) and transcriptional ($T\text{-}bet^-ROR\gamma t^{lo}$; Supporting Fig. S2C) markers. Surprisingly, a substantial subset of HCC-enriched ILC2s did not express KLRG1 (orange oval circle), a well-documented marker for mature ILC2s in the blood, mucosal tissues, and nonmucosal tissues in the resting state,[19] suggesting the existence of an HCC-derived ILC2 subtype. Furthermore, levels of known ILC2 activators, including IL-33, IL-25, and TSLP, were diminished in HCC samples (Fig. 2F and Supporting Fig. S3), indicating that the HCC-derived ILC2s might be functionally divergent from canonical ILC2s. Thus, a distinct tumor-derived ILC2 population accumulates in the HCC microenvironment.

KLRG1- ILC2s ARE TISSUE-DERIVED AND MORE PROLIFERATIVE IN HCC

We found that the HCC-induced ILC2s expressed higher CD69 levels than ILC2s from nontumoral tissue, whereas those isolated from human peripheral and portal vein blood lacked CD69 (Fig. 3A), prompting us to speculate that these HCC-accumulated ILC2s

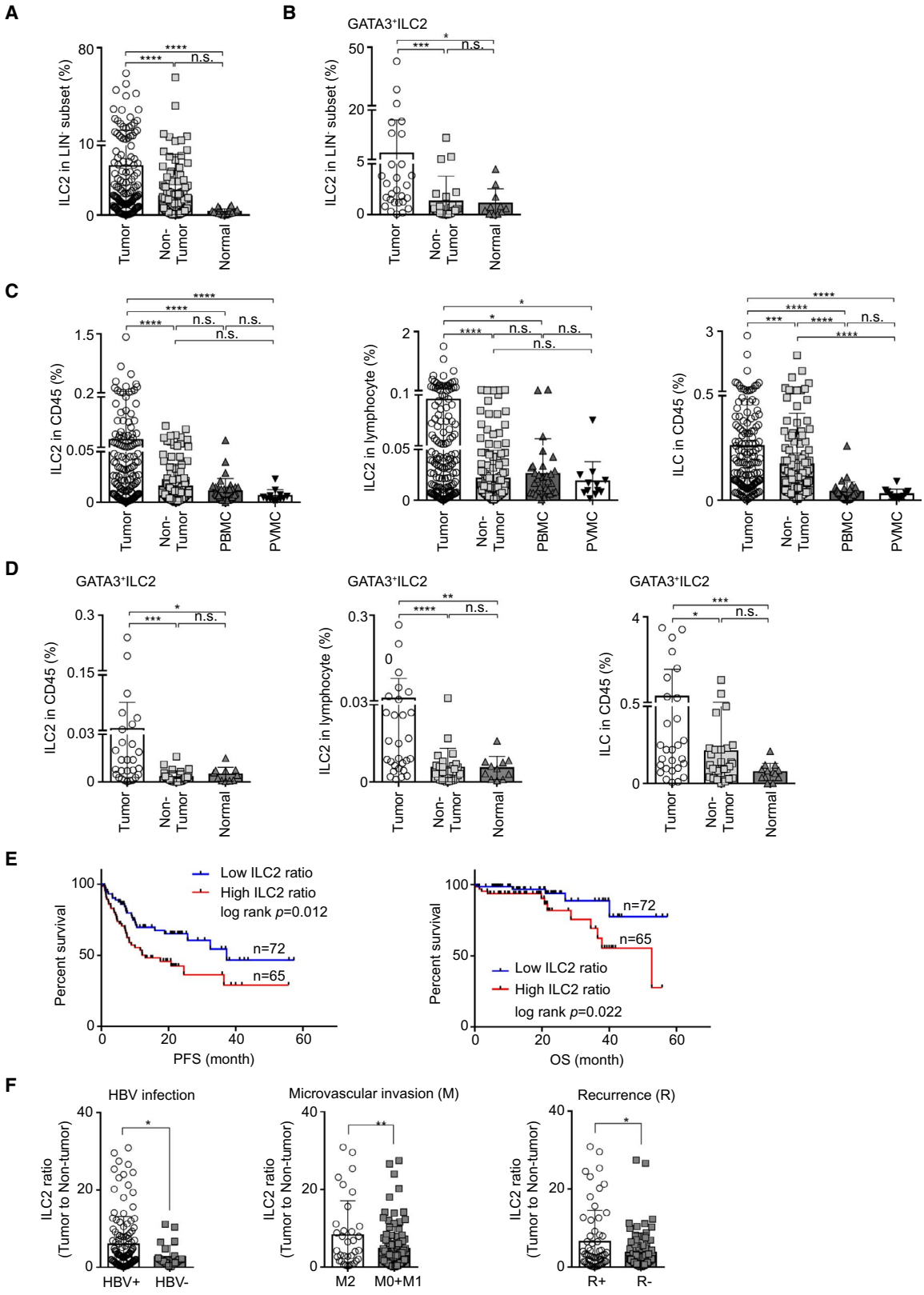
A
ILC2 in LIN- subset (%)
Tumor
Non-Tumor
Normal
B
GATA3+ILC2
ILC2 in LIN- subset (%)
C
ILC2 in CD45 (%)
ILC2 in lymphocyte (%)
ILC in CD45 (%)
PBMC
PVMC
D
GATA3+ILC2
E
Low ILC2 ratio
High ILC2 ratio
log rank p=0.012
n=72
n=65
Percent survival
PFS (month)
log rank p=0.022
OS (month)
F
HBV infection
Microvascular invasion (M)
Recurrence (R)
ILC2 ratio (Tumor to Non-tumor)
HBV+
HBV-
M2
M0+M1
R+
R-

FIG. 1. HCC-derived hepatic ILC2s correlate with HCC survival. (A) Percentages of ILC2s (gated as $CD45^+LIN^-CD127^+CRTH2^+$) in the $CD45^+LIN^-$ subsets of 150 paired tumor and nontumor tissues and 20 normal liver tissues. (B) Percentages of $CRTH2^+GATA3^+ROR\gamma t^{lo}$ ILC2s in tumor, paired nontumor tissues (n = 28), and normal liver tissues (n = 11) relative to the LIN^- subset. (C) Percentages of ILC2s in tumor, paired nontumor tissues (n = 150), and autologous peripheral blood (n = 38) and portal vein blood (n = 12) relative to the $CD45^+$ cells, lymphocytes, and ILC subsets in $CD45^+$ cells. (D) Percentages of $GATA3^+$ ILC2s in tumor, paired nontumor tissues (n = 28), and normal liver tissues (n = 11) relative to the $CD45^+$ cells, lymphocytes, and ILC subsets in $CD45^+$ cells. (E) The PFS and overall survival of low and high tumor/no-tumor ILC2 ratios. The cohort was separated based on the median value of the tumor/nontumor ILC2 ratio. (F) Potential correlations of tumor/nontumor ILC2 ratios with HBV infection, microvascular invasion, and recurrence. Statistical analysis was performed using the Mann-Whitney U test (A-D,F) or Kaplan-Meier curves using the log-rank test (E). $^*P < 0.05$, $^{**}P < 0.01$, $^{***}P < 0.001$, and $^{****}P < 0.0001$. Abbreviations: n.s., not significant; OS, overall survival.

were derived from local tissues, not the circulation. From the transcriptomic data of ILC2s sorted from the paired HCC and nontumoral tissues, we detected high expression levels of certain core tissue residency genes in the tumor-derived ILC2s, whereas that of nontumoral tissues had a transcriptomic signature similar to circulating naïve $CD3^+$ T cells (Fig. 3B, left; and Supporting Table S7), which were inhibited in the HCC-derived ILC2s (Fig. 3B, right; Supporting Table S7). Immunofluorescence assays showed that hepatic ILC2s were distant from the circulating T ($CD3^+$ $CD5^+$ $TCR\alpha/\beta^+$ $TCR\gamma/\delta^+$) cell aggregation pool, which was thought to reside either in the central vein or the portal area in the liver, indicating a noncirculating characteristic of hepatic ILC2s in tumors (Fig. 3C).

Flow cytometry confirmed an increased proportion of $KLGR1^-$ ILC2s in HCC tissue than in nontumoral tissue and PBMCs (Fig. 3D). To study the origin of $KLGR1^-$ ILC2s in HCC, we co-cultured hepatic ILC2s ($CD45^+LIN^-CD127^+ST2^+$) obtained and identified from recombinant murine IL-33-treated mice (Supporting Fig. S4) directly with Hepa1-6 cells, and observed a significant decrease in KLRG1 in the former, whereas co-culture in Transwell inserts without direct cell-to-cell contact had no effect (Supporting Fig. S5). Interestingly, KLRG1 expression on ILC2s was also unaffected when co-cultured with AML-12 cells (Supporting Fig. S5). KLRG1 signaling is mediated by an interaction with cadherin, particularly E-cadherin; therefore, we investigated their relationship in ILC2s. Corroboratively, E-cadherin was absent from Hepa1-6 and H22 mouse HCC cell lines (Supporting Fig. S6A) and was decreased in most human HCC cell lines (Supporting Fig. S6B). E-cadherin expression, represented by fragments per kilobase million values from the GEO database, in HCC were lower compared with that of nontumoral tissues (Supporting Fig. S6C), and the protein level was lower in a higher proportion of HCC samples (Supporting Fig. S6D). Importantly, overexpression of *Cdh1* (encoding E-cadherin) in Hepa1-6 cells maintained (Supporting Fig. S8A,B), whereas knockout of *Cdh1* in AML-12 cells decreased, KLRG1 expression in co-cultured ILC2s (Supporting Fig. S7C,D), which helped to determine the interactions between E-cadherin and KLRG1. Further verified in HCC samples shown in Fig. 3C, the positive correlation between E-cadherin expression and the $KLRG1^+$ILC2 ratio (Supporting Fig. S8) confirmed the relevance of these two markers.

KLRG1 could induce inhibitory signaling; therefore, we hypothesized that KLRG1 controls the proliferation of hepatic ILC2s. Indeed, we observed a positive correlation between the proportion of $KLRG1^-$ hepatic ILC2s and the total ILC2s of hepatic lymphocytes (Fig. 3E). Human primary hepatic ILC2s isolated from tumor tissues displayed a typical lymphoid morphology, expressed GATA3 and IL-13, and could proliferate dramatically *in vitro* in the presence of IL-2 and IL-33 (Supporting Fig. S9). $KLRG1^-$ ILC2s isolated from HCC tissues showed significantly higher proliferation rates compared with $KLRG1^+$ ILC2s when co-cultured with OP9 bone marrow stromal cells in the presence of 10 ng/mL IL-2, IL-7, IL-25, and IL-33 (Fig. 3F, left), leading to a drastic increase in their total numbers (Fig. 3F, right). Taken together, the self-renewal capacity of HCC-derived ILC2s contributes to their accumulation at tumor sites.

HCC-DERIVED HEPATIC ILC2s PRODUCE NEUTROPHIL ATTRACTANTS CXCL2, CXCL8, AND Th2 CYTOKINE IL-13

Transcriptome analysis of hepatic ILC2s from paired HCC and nontumor tissues showed a significant enrichment of cell chemotaxis function, which was reflected in the up-regulation of the CXC

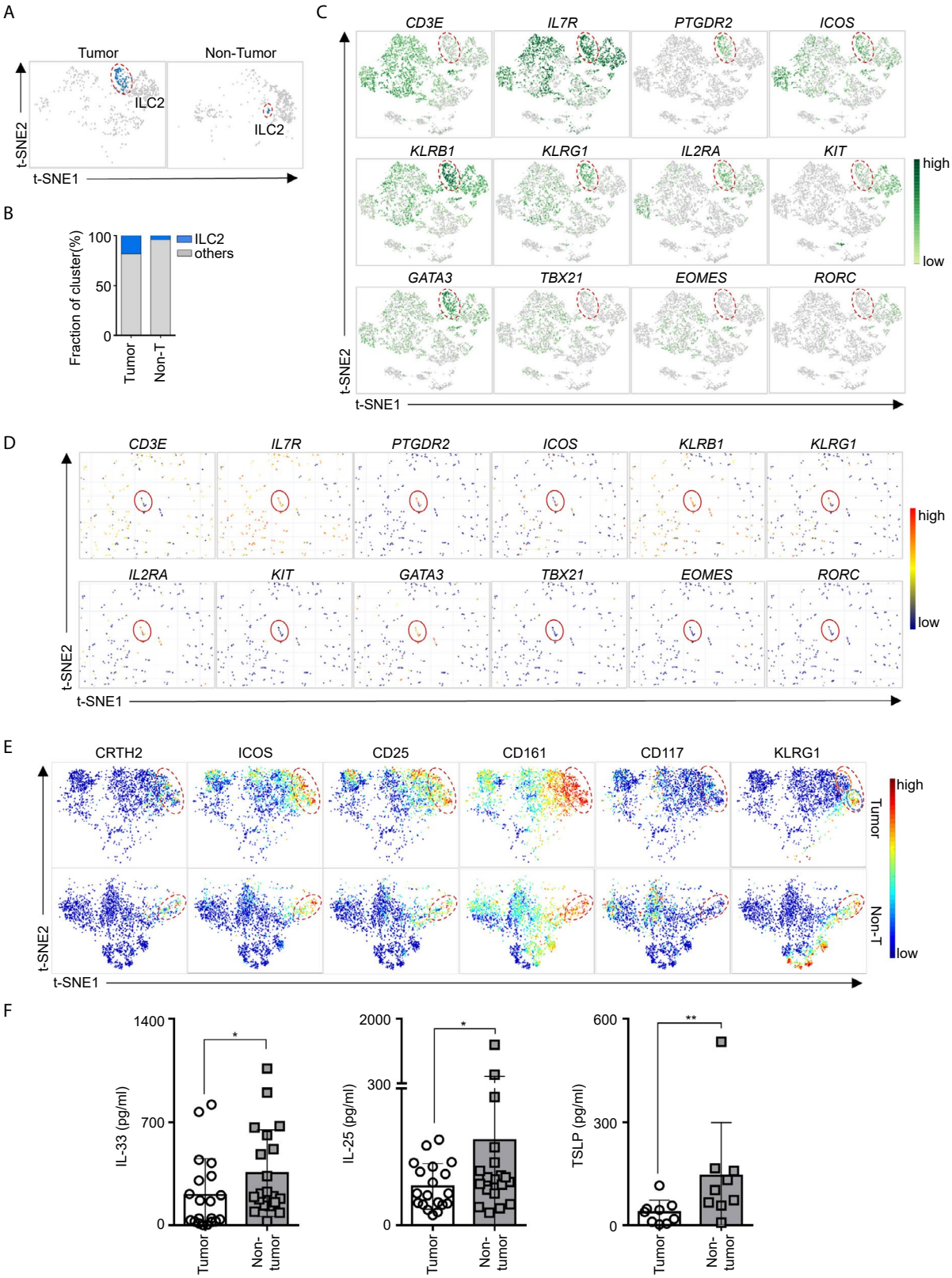
A
Tumor
Non-Tumor
ILC2
ILC2
t-SNE2
t-SNE1
B
Fraction of cluster(%)
100
50
0
ILC2
others
Tumor
Non-T
C
CD3E
IL7R
PTGDR2
ICOS
KLRB1
KLRG1
IL2RA
KIT
GATA3
TBX21
EOMES
RORC
high
low
t-SNE2
t-SNE1
D
CD3E
IL7R
PTGDR2
ICOS
KLRB1
KLRG1
IL2RA
KIT
GATA3
TBX21
EOMES
RORC
high
low
t-SNE2
t-SNE1
E
CRTH2
ICOS
CD25
CD161
CD117
KLRG1
Tumor
Non-T
high
low
t-SNE2
t-SNE1
F
IL-33 (pg/ml)
1400
700
0
*
Tumor
Non-tumor
IL-25 (pg/ml)
2000
300
0
*
Tumor
Non-tumor
TSLP (pg/ml)
600
300
0
**
Tumor
Non-tumor

FIG. 2. The phenotype of hepatic ILC2s in tumor and nontumoral tissue. (A) Two-dimensional visualization of single-cell cluster of ILC2s (gated on LIN^-*IL7R*$^+$*PTGDR2*$^+$*GATA3*$^+$) in HCC and nontumoral tissue by t-SNE, indicated by a red dotted circle. Each dot corresponds to one single cell. (B) The proportion of ILC2s across LIN^-IL7R^+ cell subsets in paired HCC and nontumoral tissue (blue, ILC2s; gray, other cells). (C) ILC2 cluster in t-SNE plots (every single cell captured for sequencing was included; T = 5,585 cells, n = 5,116 cells) marked by the mRNA expression of surface markers (*IL-7R*, *PTGDR2*, *ICOS*, *KLRB1*, *KLRG1*, *IL-2RA*, and *KIT*) and transcription factors (*GATA3*, *TBX21*, *EOMES*, and *RORC*) (green, high; gray, low). (D) Magnified t-SNE visualized plots showing the expression of selected identification and exclusion marker genes for ILC2s (Supporting Fig. S2A,B) from scRNA-seq data from the CNGB Nucleotide Sequence Archive (CNP0000650) (red, high; blue, low). (E) Visualized t-SNE map of cells from tumor and nontumor tissue pregated on $CD45^+LIN^-CD127^+$ cells from mass cytometry analysis. Normalized expression intensities of related surface markers were calculated and overlaid on the t-SNE plot (red, high; blue, low). Orange and blue oval dotted circles indicate $KLRG1^-$ and $KLRG1^+$ cells, respectively. Data shown are from 3 patients. (F) Concentration of IL-33 (n = 18), IL-25 (n = 18), and TSLP (n = 9) in the supernatants of liver tissues as determined using ELISA. Statistical analysis was performed using a two-tailed paired Student *t* test. Data are shown as the mean ± SD. $^*P < 0.05$, $^{**}P < 0.01$. Abbreviations: *EOMES,* eomesodermin; *KLRB1*, killer cell lectin like receptor B1; *RORC,* RAR related orphan receptor C; *TBX21*, T-box transcription factor 21.

chemokine family members, especially *CXCL2* and *CXCL8*, in HCC-associated hepatic ILC2s (Fig. 4A). GSEA further revealed that the difference between tumor and nontumoral ILC2s resembled that between lipopolysaccharide-treated or control-treated monocytes (normalized enrichment score [NES] = 1.647, *p*.adjust = 0.011; Fig. 4B). As a dominant member of Th2 cytokines, IL-13, along with other secretory factors, drove a significant enrichment of cytokine and cytokine receptor interaction–related genes in HCC-derived ILC2s (NES = 1.56, *p*.adjust = 0.016; Fig. 4C). After treatment with a leukocyte stimulation cocktail *in vitro*, using the $CD127^+CRTH2^-GATA3^-$ subset as a control, we confirmed that HCC-derived ILC2s secreted higher levels of IL-13 and CXCL8 (IL-8) than those from nontumoral tissues (Fig. 4D). Accordingly, the frequency of HCC-induced ILC2s correlated positively with the number of neutrophils relative to the $CD45^+$ population (Fig. 4E), because both CXCL2 and CXCL8 chemokines are powerful neutrophil attractants. After co-culture with AML-12 cells, ILC2 expression of *Il-13* and *Cxcl2* was strongly inhibited, compared to those cultured with Hepa1-6 cells (Fig. 4F). Taken together, HCC-derived ILC2s are functionally enhanced.

LOSS OF KLRG1 CAUSES ENHANCED PROLIFERATION OF ILC2s, ATTRACTS NEUTROPHILS, AND INDUCES AN IMMUNOSUPPRESSIVE PHENOTYPE

We then validated these findings in an established c-Myc/NRas-induced murine HCC model,[16] in which we detected a higher frequency and larger number of $CD45^+LIN^-CD127^+GATA3^+ROR\gamma t^-$ ILC2s in the tumor-bearing livers (Supporting Figs. S10 and S11), similar to the observations in human specimens. Additionally, the c-Myc/NRas-induced HCC also harbored fewer $KLRG1^+$ ILC2s (Fig. 5A). An *in vivo* BrdU assay showed that hepatic $KLRG1^-$ ILC2s exhibited a significantly stronger proliferative capacity than the $KLRG1^+$ ILC2s in HCC tissues (Fig. 5B). To determine whether KLRG1 is a key factor modulating ILC2 proliferation, we generated *Klrg1* knockout (ILC2-CRISPR-KLRG1) and overexpressing (ILC2-PCDH-KLRG1) ILC2s (Supporting Fig. S12) and cultured them with 10 ng/mL IL-2/IL-33. *Klrg1* overexpression suppressed, whereas deprivation of KLRG1 inhibitory signaling promoted, ILC2 proliferation (Fig. 5C).

We next determined the effect of *Klrg1* on the expression levels of Th2 cytokines and *Cxcl2* in murine ILC2s, because the RayBio mouse cytokine antibody array (Mouse 23-plex) showed that isolated murine ILC2s primarily produced Th2 cytokines (Supporting Fig. S13), and the transcriptome data indicated that human HCC-induced ILC2s expressed equal levels of *IL-13*, *CXCL2*, and *CXCL8* (Supporting Fig. S14). The *CXCL8* gene was not examined because it is absent in mice.[20] *Klrg1* overexpression downregulated *Il-13* and *Cxcl2* mRNA levels, whereas its knockout enhanced the production ability of ILC2s (Fig. 5D). A chemotaxis assay showed that the conditioned medium (CM) of ILC2-PCDH-KLRG1 cells decreased neutrophil migration significantly, whereas ILC2-CRISPR-KLRG1 CM promoted chemotaxis (Supporting Fig. S15), in accordance with their chemokine production capacity. Furthermore,

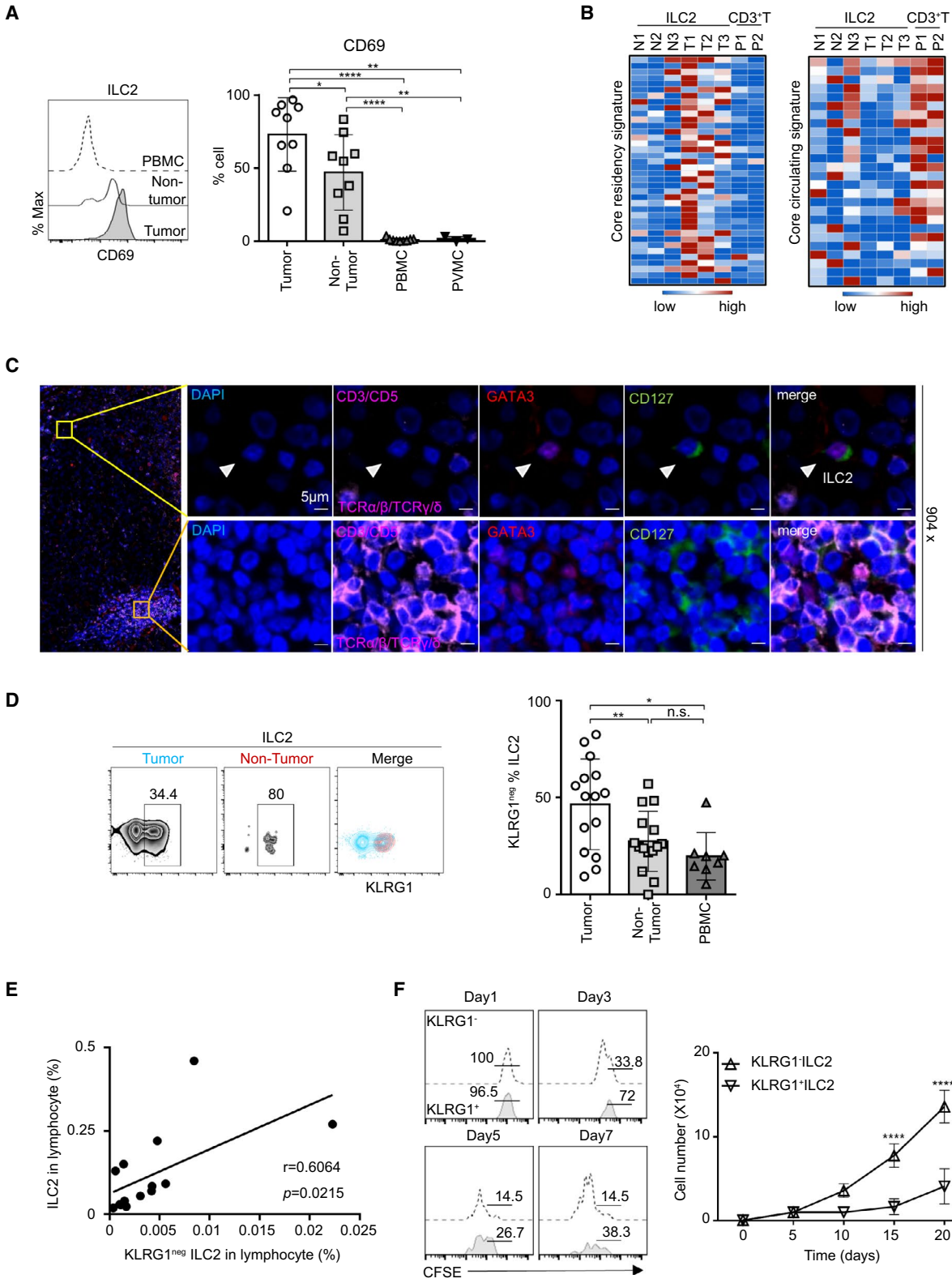
A
ILC2
PBMC
Non-tumor
Tumor
% Max
CD69
CD69
% cell
Tumor
Non-Tumor
PBMC
PVMC
B
ILC2
CD3+T
N1 N2 N3 T1 T2 T3 P1 P2
Core residency signature
Core circulating signature
low
high
C
DAPI
CD3/CD5
GATA3
CD127
merge
ILC2
5μm
TCRα/β/TCRγ/δ
904 x
D
ILC2
Tumor
Non-Tumor
Merge
34.4
80
KLRG1
KLRG1neg % ILC2
n.s.
Tumor
Non-Tumor
PBMC
E
ILC2 in lymphocyte (%)
r=0.6064
p=0.0215
KLRG1neg ILC2 in lymphocyte (%)
F
Day1
Day3
Day5
Day7
KLRG1-
KLRG1+
100
96.5
33.8
72
14.5
26.7
14.5
38.3
CFSE
KLRG1-ILC2
KLRG1+ILC2
Cell number (X10⁴)
Time (days)

FIG. 3. HCC-originated hepatic ILC2s are tissue-derived and more proliferative. (A) Representative flow cytometry histogram showing CD69 expression in ILC2s from tumor and nontumor tissues and peripheral blood from 1 representative patient (left panel). Percentage of $CD69^+$ ILC2s from liver tissues (tumor and nontumor) and peripheral blood of 9 patients and the portal vein blood of 3 patients (right panel). (B) Relative expression of 38 core tissue-resident and 26 core circulating genes in ILC2s derived from HCC, nontumor tissue, and peripheral blood naïve $CD3^+$ T cells (blue, low; red, high; see Supporting Table S7 for gene list). (C) Representative immunofluorescence images of human HCC tissue sections stained with antibodies against CD3, CD5, TCRα/β, TCRγ/δ (pink), CD127 (green), and GATA3 (red), and stained with 4′,6-diamidino-2-phenylindole (blue). Magnification, ×904. Cells marked by white arrows are ILC2s. (D) Representative flow cytometry plots showing KLRG1 expression in ILC2s from tumor and paired nontumor liver tissue (left panel). Percentage of KLRG1 expression in ILC2s from tumor, paired nontumor liver tissues (n = 15), and peripheral blood (n = 8) pregated on $CD45^+LIN^-CD127^+CRTH2^+$ cells (right panel). (E) Correlation of the percentage of $KLRG1^-$ hepatic ILC2s to that of the total hepatic ILC2s in lymphocytes from HCC tissues (n = 15). (F) Proliferation of the sorted $KLRG1^-$ ILC2s and $KLRG1^+$ ILC2s co-cultured with OP9 cells. CFSE-labeled cells were detected using flow cytometry at days 1, 3, 5, and 7 (left panel). The number of $KLRG1^-$ and $KLRG1^+$ ILC2s recorded on days 5, 10, 15, and 20 (right panel). Statistical analysis was performed using the Mann-Whitney U test (A), the Pearson correlation test (E), two-way ANOVA (F), or a two-tailed unpaired (D) Student *t* test. $^*P < 0.05$, $^{**}P < 0.01$, $^{****}P < 0.0001$. Abbreviations: DAPI, 4′,6-diamidino-2-phenylindole; N, nontumor ILC2s; P, PBMC-naïve $CD3^+$ T cells; T, tumor ILC2s.

the application of anti-CXCL2 antibodies inhibited chemotaxis significantly in both groups (Supporting Fig. S16). The results were also verified using hepatic ILC2s isolated from human HCC: Stimulation of KLRG1 signaling using E-cadherin hindered cytokine and chemokine expression, and neutrophil attraction (Supporting Fig. S17). The ILC2 CM also induced an immunosuppressive cytokine profile in neutrophils (Supporting Fig. S18), likely by up-regulating *Arg1* through Th2 cytokines. Consistent with the regulation of *Il-13* by *Klrg1*, *Arg1* levels were up-regulated by the ILC2-CRISPR-KLRG1 CM and down-regulated by the ILC2-PCDH-KLRG1 CM (Fig 5E). In addition, neutrophils pre-incubated with the CMs of ILC2-CRISPR-KLRG1 or ILC2-PCDH-KLRG1 significantly decreased or enhanced the proliferation and cytotoxicity of the co-cultured $CD8^+$ T cells, respectively (Fig. 5F and Supporting Fig. S19). Taken together, these results showed that $KLRG1^-$ hepatic ILC2s induce an immunosuppressive TME.

ILC2s PROMOTE HCC DEVELOPMENT THROUGH CXCL2/NEUTROPHILS *IN VIVO*

We then confirmed our speculation about the role of the ILC2/CXCL2/neutrophil pathway in HCC development *in vivo*. From the normal liver, early stage, and late stage of HCC in the mouse model, the ratio and absolute number of ILC2s, *Cxcl2* expression, and the neutrophil infiltration rate increased with increasing tumor burden. Meanwhile, in the tissue that lost E-cadherin expression, the KLRG1 expression of ILC2s decreased significantly (Supporting Fig. S20). We adoptively transferred $CD45.1^+$ ILC2s into tumor-bearing and control mice of the CD45.2 strain, and found that at 3 days following injection, the transferred $CD45.1^+$ ILC2s with diminished KLRG1 expression were detectable in the tumor sites (Supporting Fig. S21). Fourteen days after establishing the *in situ* HCC model, tumor-bearing mice were injected with ILC2s or PBS every 3 days. Transferring ILC2s resulted in significantly increased neutrophils, arginase expression, and tumor burden (Fig. 6A and Supporting Fig. S22). To test the contribution of KLRG1, we transferred ILC2s with either *Klrg1* overexpression or knockout, and observed elevated neutrophils, higher arginase expression, and a heavier tumor burden in the ILC2 *Klrg1* knockout group (Fig. 6B and Supporting Fig. S23). Furthermore, after ILC2-CRISPR-CXCL2 cells were generated and purified (Supporting Fig. S24), the tumor-promoting ability of ILC2s lacking CXCL2 expression was demonstrated to be markedly reduced, together with decreased neutrophil accumulation (Fig. 6C and Supporting Fig. S25A), although there were no differences in arginase expression, which might reflect the unaffected IL-13 levels (Supporting Fig. S25B). Finally, antibody-mediated depletion of neutrophils (Fig. 6D) in the tumor-bearing mice injected with ILC2s alleviated the tumor burden (Fig. 6E and Supporting Fig S26) and partially restored the $CD8^+$ T-cell population (Fig. 6F). Therefore, ILC2s promote HCC development through the creation of a neutrophil-mediated suppressive microenvironment.

Discussion

HCC is a heterogeneous malignancy with a highly complex immune microenvironment, which induces both anti-tumor and pro-tumor responses

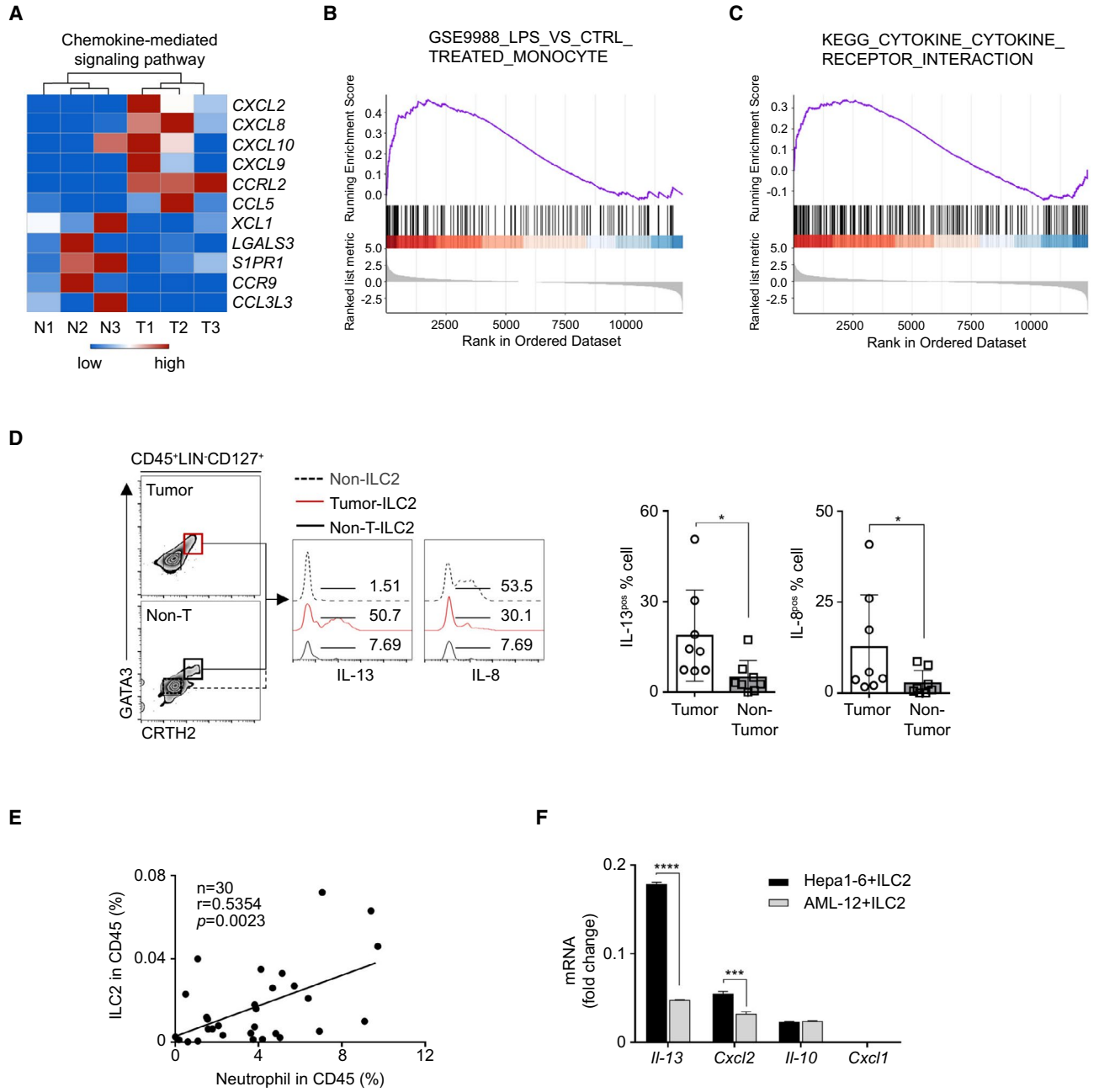

FIG. 4. HCC-derived ILC2s express higher levels of CXCL2, CXCL8, and IL-13. (A) Relative expression of chemotaxis signature genes in paired tumor and nontumor hepatic ILC2s isolated from 3 patients. Data were derived from RNA-seq. (B,C) GSEA analysis showing the genes from HCC-derived ILC2s enriched primarily in lipopolysaccharide-stimulated monocytes (B) and interactions between cytokines and receptors (C). (D) Representative cytometry plots (left panel) and percentage analysis (n = 8) of IL-13 and IL-8 (CXCL8) expression from tumor-originated ILC2s (red), nontumoral ILC2s (solid), and non-ILC2s ($CRTH2^{-}GATA3^{-}$, dotted). (E) Correlation of the percentage of total hepatic ILC2s to that of $CD45^{+}CD11b^{+}CD66b^{+}$ neutrophils (n = 30). (F) 4×10^{4} murine ILC2s were co-cultured with Hepa1-6 or AML-12, respectively, for 3 days. Relative mRNA expression of *Il-13*, *Cxcl2*, *Il-10*, and *Cxcl1* in murine ILC2s isolated from the co-culture system, as examined using quantitative real-time PCR. Statistical analysis was performed using a two-tailed paired Student *t* test (D,F) and Pearson correlation test (E). $^{*}P < 0.05$, $^{***}P < 0.001$, $^{****}P < 0.0001$. Abbreviations: CTRL, Control CCRL2, C-C motif chemokine receptor like 2; CCL5 C-C motif chemokine ligand 5; CCR9 C-C motif chemokine receptor 9; CCL3L3 C-C motif chemokine ligand 3 like 3; CRTH2 C-C Chemo attractor Receptor-homologous molecule expressed on Th2 cells; KEGG, Kyoto Encyclopedia of Genes and Genomes; LGALS3, lectin, galactoside-binding, soluble, 3; LPS, lipopolysaccharide; LGALS3, lectin, galacotoside-binding, soluble, 3; Non-T-ILC2, nontumor-ILC2; S1PR1, Sphingoine-1-phosphate receptor 1; XCL 1; X-C motif chemokine ligand 1.

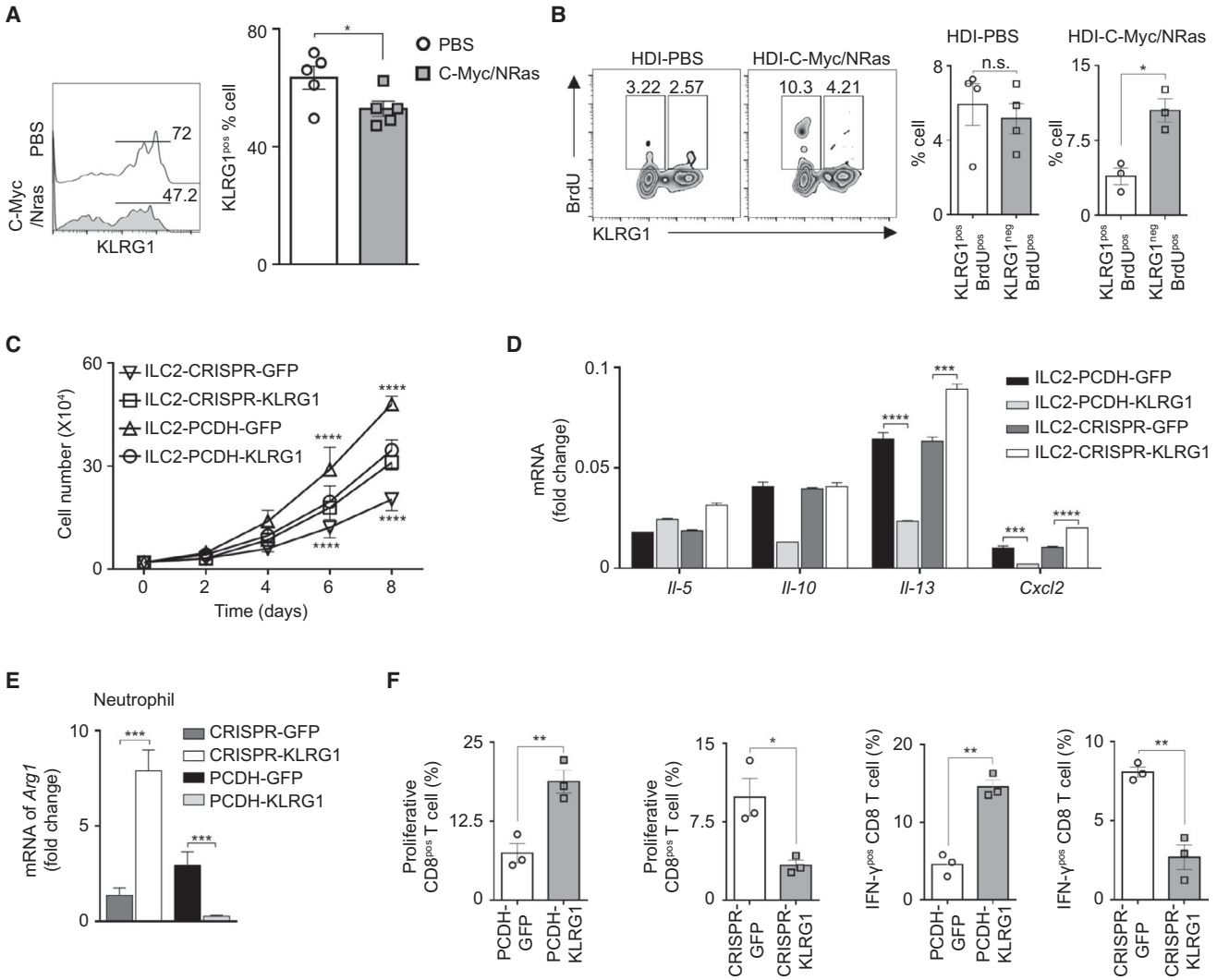

FIG. 5. KLRG1$^-$ ILC2s promote HCC by self-proliferation, and attracting and inducing an immunosuppressive phenotype in neutrophils. (A) KLRG1 expression in hepatic ILC2s from the c-Myc/Nras-induced HCC model and control mice. (B) Proliferation of KLRG1$^-$ ILC2s and KLRG1$^+$ ILC2s determined by BrdU incorporation in oncogene-induced liver tumors and controls. (C) Proliferation curves of ILC2s-CRISPR-GFP, ILC2-CRISPR-KLRG1, ILC2-PCDH-GFP, and ILC2-PCDH-KLRG1 cells that were cultured *in vitro* with 10 ng/mL IL-2 and IL-33 for 8 days. (D) Relative mRNA levels of *Il-5*, *Il-10*, *Il-13*, and *Cxcl2* in ILC2-CRISPR-GFP, ILC2-CRISPR-KLRG1, ILC2-PCDH-GFP, and ILC2-PCDH-KLRG1 cells. (E) Relative expression of *Arg1* in neutrophils cultured in the CM of ILC2-CRISPR-GFP, ILC2-CRISPR-KLRG1, ILC2-PCDH-GFP, and ILC2-PCDH-KLRG1 cells. (F) Percentage of proliferative CD8$^+$ T cells labeled with CFSE and interferon-γ-producing CD8$^+$ T cells detected using flow cytometry after 2 days of co-culture, with neutrophils pretreated with the CM of ILC2-PCDH-KLRG, ILC2-CRISPR-KLRG1, and related control cells. Statistical analysis was performed using two-way ANOVA (C) or two-tailed unpaired Student *t* test (A-B,D-F). **P* < 0.05, ***P* < 0.01, ****P* < 0.001, *****P* < 0.0001. Abbreviation: GFP, green fluorescent protein; HDI, hydrodynamic injection.

under distinct circumstances. We observed a higher proportion of hepatic ILC2s in HCC relative to nontumoral and normal liver tissues. Different ILCs show substantial plasticity, and reversible trans-differentiation between ILC1s and ILC3s is frequently observed.[21] Previously, we showed that Notch signaling converted natural ILC2s into inflammatory ILC2s that displayed dual ILC2/ILC3 capabilities.[22] The present study revealed a significant increase in the overall ILC proportion among HCC tissue hematopoietic cells relative to the paired nontumoral liver tissues, strongly

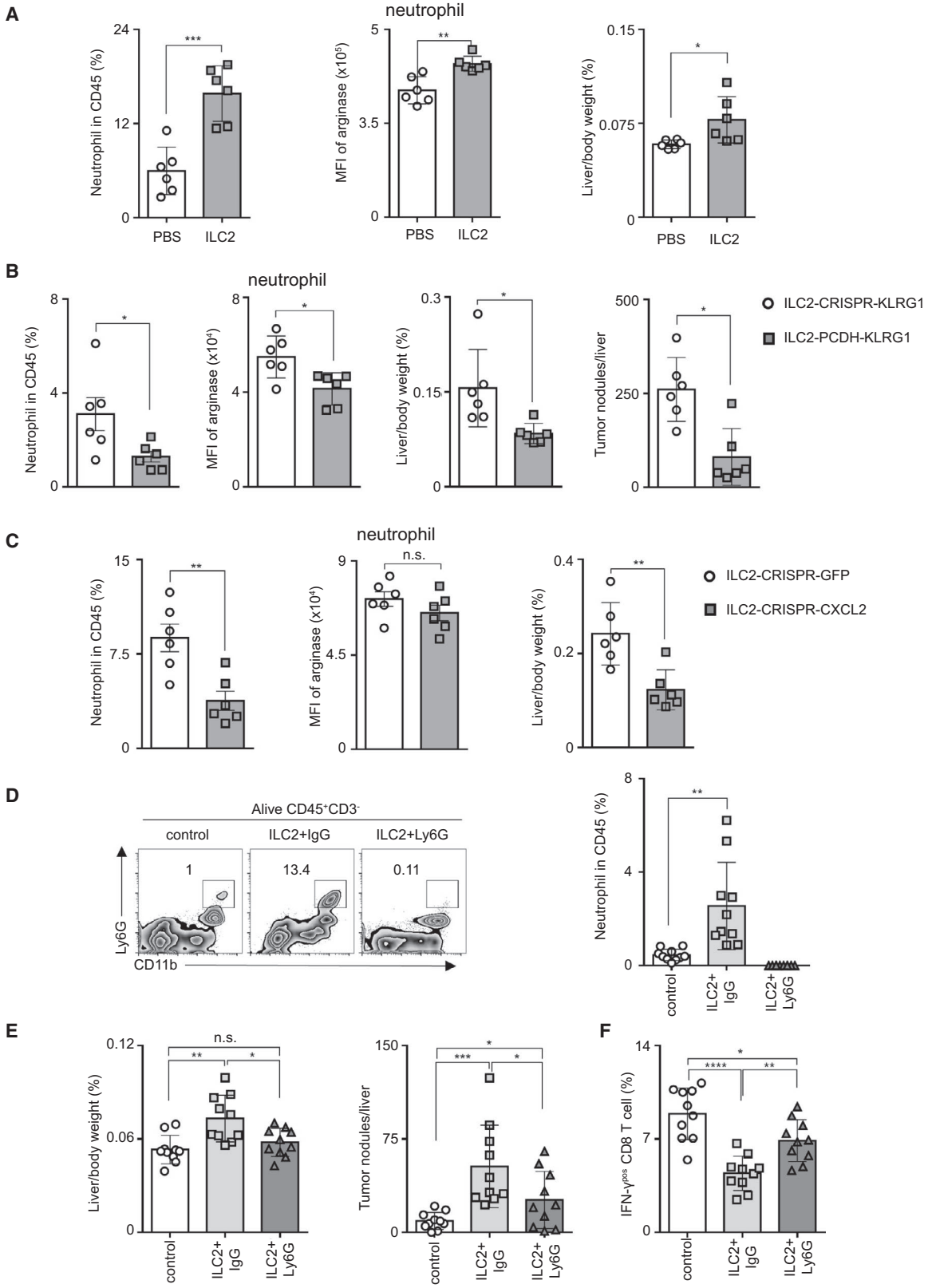
A
neutrophil
Neutrophil in CD45 (%)
MFI of arginase (x10⁵)
Liver/body weight (%)
PBS
ILC2
B
neutrophil
Neutrophil in CD45 (%)
MFI of arginase (x10⁴)
Liver/body weight (%)
Tumor nodules/liver
ILC2-CRISPR-KLRG1
ILC2-PCDH-KLRG1
C
neutrophil
n.s.
Neutrophil in CD45 (%)
MFI of arginase (x10⁴)
Liver/body weight (%)
ILC2-CRISPR-GFP
ILC2-CRISPR-CXCL2
D
Alive CD45⁺CD3⁻
control
ILC2+IgG
ILC2+Ly6G
1
13.4
0.11
Ly6G
CD11b
Neutrophil in CD45 (%)
control
ILC2+ IgG
ILC2+ Ly6G
E
n.s.
Liver/body weight (%)
Tumor nodules/liver
F
IFN-γ^pos CD8 T cell (%)

FIG. 6. ILC2s promote HCC development through CXCL2/neutrophils in vivo. (A) Murine *in situ* HCC models were established through hydrodynamic injection of oncogene plasmids. Murine ILC2s and PBS were injected into the caudal vein every 3 days. The percentage of neutrophils in $CD45^+$ cells, MFI of arginase in neutrophils, and liver weight relative to body weight are shown. (B) HCC model mice were treated with injection of ILC2-CRISPR-KLRG1 or ILC2-PCDH-KLRG1 cells. The percentage of neutrophils in $CD45^+$ cells, mean fluorescence intensity (MFI) of arginase in neutrophils, the liver/body weight ratio, and liver tumor nodules were calculated. (C) HCC model mice were injected with ILC2-CRISPR-GFP or ILC2-CRISPR-CXCL2 cells. The percentage of neutrophils in $CD45^+$ cells, MFI of arginase in neutrophils, and liver/body weight ratio are shown. (D) ILC2-treated HCC mice were injected peritoneally with 300 μg of anti-Ly6G or anti-IgG antibody every 2 days. Representative flow cytometry plots (gated on alive $CD45^+CD3^-$) showing the neutrophil ($CD11b^+Ly6G^{hi}$) depletion efficiency and the percentage of neutrophils in $CD45^+$ cells. (E) Tumor burden was measured as liver/body weight and the number of liver tumor nodules. (F) The percentage of interferon-γ^+ CD8 T cells are shown. Statistical analysis was performed using a two-tailed unpaired Student *t* test. $^*P < 0.05$, $^{**}P < 0.01$, $^{***}P < 0.001$, $^{****}P < 0.0001$. Abbreviation: IFN-γ, interferon-γ.

indicating active proliferation and self-renewal of hepatic ILC2s in the HCC microenvironment, rather than trans-differentiation from other subsets. Studies have shown that ILCs are tissue-sessile cells with limited migratory abilities.[23] Consistent with this, we observed similar ILC2 proportions between peripheral and portal vein blood, indicating the lack of migration into HCC tissues. Comparisons between HCC-induced hepatic ILC2s and peripheral naive $CD3^+$ T cells confirmed that the increased ILC2s levels in HCC originated within the tumor.

The role of ILC2s in tumor initiation and progression is ambiguous, partly because of the complex TME. However, proliferative ILC2s have a pro-tumorigenic role in gastric,[24] breast,[25] and bladder[26] cancers. Here, we report an immunosuppressive role of hepatic ILC2s in HCC. The ILC2-initiating cytokines IL-25, IL-33, and TSLP, verified by numerous previous studies, appear not to be potent activators of these hepatic ILC2s under HCC circumstance. Jeffery et al.[27] reported that intrahepatic ILC2s expressed low levels of the IL-33 receptor, ST2, as confirmed by mass cytometry, which also showed lower levels of IL-17RB and TSLPR in hepatic ILC2s (data not shown). Consistently, the levels of IL-25, IL-33, and TSLP in HCC were significantly diminished compared with those in the paired nontumoral tissues. Another study also identified ILC2-like cells that were independent of IL-33,[28] indicating the existence of tissue-specific pathways that determine ILC2 phenotype and function.

The HCC-induced ILC2s were polarized to a less-mature $KLRG1^-$ phenotype, showing enhanced self-renewal and proliferation. KLRG1 is expressed primarily by mature natural killer (NK) cells[29] and terminally differentiated T cells,[30] and correlates with reduced proliferation, increased apoptosis, and impaired IFN-γ secretion in NK cells.[31] KLRG1 interaction with tissue-specific E-cadherin could be an essential mechanism to maintain tissue homeostasis by ameliorating ILC2-Th2 cytokine-driven inflammation. Therefore, we hypothesized that low hepatic tumor ILC2 KLRG1 expression might result from diminished HCC cell E-cadherin expression. Without E-cadherin stimulation, hepatic ILC2s escape from KLRG1-mediated inhibitory signaling. Moreover, low ST2 expression on hepatic ILC2s and/or low IL-33 release into the HCC microenvironment augmented KLRG1 loss, because IL-33 is known to up-regulate KLRG1 in ILC2s.[32] These $KLRG1^-$ ILC2s were highly proliferative compared with the $KLRG1^+$ ILC2s in human and murine HCC, supporting our hypothesis that enriched hepatic ILC2s in HCC result from self-renewal rather than trans-differentiation across ILC subgroups or migration from other tissues.

In addition to Th2 cytokines, ILC2s also produce amphiregulin,[33] granulocyte-macrophage colony-stimulating factor, CXCL1, and CXCL2.[34] We found that the HCC-derived ILC2s expressed higher levels of CXCL2 and CXCL8, which are potently chemotactic for neutrophils.[35,36] The expansion of hepatic $KLRG1^-$ ILC2s attracted neutrophils to the tumor site through enhanced *CXCL2* expression, confirming that innate lymphoid cells are important for neutrophil attraction, in addition to known epithelial, endothelial, or myeloid cells. In mouse lungs following severe trauma, IL-33-mediated IL-5 secretion from ILC2s induces neutrophil IL-5 production,[14] and in the liver of a mouse hepatitis model, ILC2s induced immunosuppressive neutrophils through IL-33-mediated IL-13 expression.[10] These interactions showed that the functional changes of neutrophils are

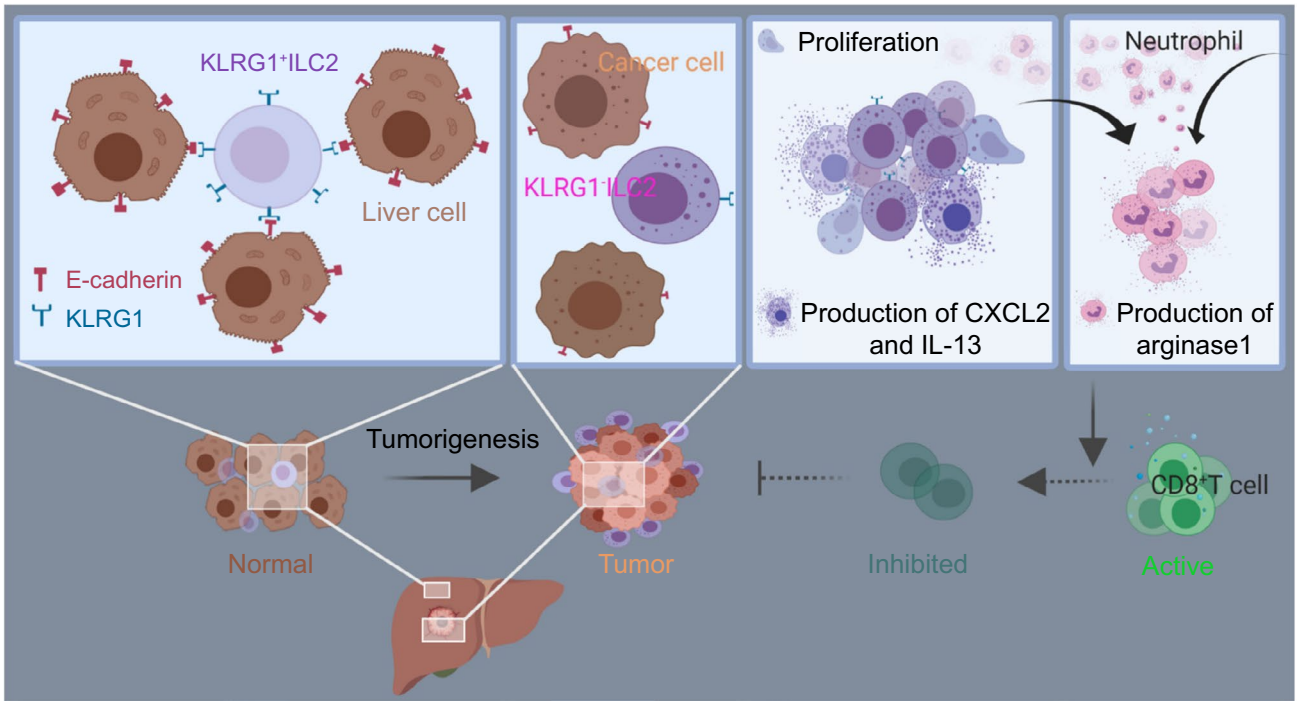

FIG. 7. Schematic model depicting the HCC-derived ILC2s inducing a suppressive immune microenvironment in HCC. When mediated by HCC with diminished E-cadherin expression, ILC2s were relieved from suppression of KLRG1 signaling by down-regulated KLRG1. Through acquisition of enhanced capacity of self-renewing as well as secreting IL-13 and CXCL2/CXCL8, ILC2s were capable of recruiting and changing neutrophils into immunosuppressive ones, to finally form an immunosuppressive microenvironment.

mediated by IL-33; however, neither of them involved neutrophil recruitment. ILC2s were also interact with other immune cells in the TME, either by secreting IL-13 to induce suppressive monocytic-myeloid derived cells,[26] or through the programmed death ligand 1/programmed death-1 (PD-1) interaction that inhibits T cells.[37] Contrastingly, recent research showed that in pancreatic ductal adenocarcinoma, IL-33-mediated ILC2s amplify PD-1 blockade and activate $CD8^+$ T cells by recruiting $CD103^+$ dendritic cells to enhance antitumor immunity.[38] Therefore, there are several other pathways through which hepatic ILC2s might shape the tumor milieu. In the present study, hepatic $KLRG1^-$ ILC2s induced immunosuppressive phenotypes of neutrophils, and the depletion of CXCL2 and neutrophils could reduce the liver tumor burden in mice partially.

To summarize, we identified a tumor tissue–derived $KLRG1^-$ hepatic ILC2 subset that was enriched in HCC and showed enhanced self-renewal. The $KLRG1^-$ ILC2/CXCL2/neutrophil axis in HCC induces an immunosuppressive microenvironment (Fig. 7). The abundance of hepatic ILC2s in HCC is associated with tumor recurrence, and correlate with poor survival of HCC. Our findings provide insights into the role of innate lymphoid cells in HCC progression, and suggest hepatic ILC2s as an attractive target for HCC immunotherapy.

Acknowledgement: The authors thank Prof. Xing Huang and Jianpeng Sheng from the First Affiliated Hospital of Zhejiang University School of Medicine for providing professional advice. They also acknowledge Dr. Xiazhen Yu, Qi Chen, Jian Zhang, Liang Wen, Yinan Shen, and Enliang Li for their technical support.

Author Contributions: X.X., L.Y., Q.Z., and T.L. contributed to the study concept and design. X.X., L.Y., and Q.Z. contributed to the analysis and interpretation of data. X.X., Q.Z., H.S., and X.Z. contributed to the methodology. X.X. and L.Y. contributed to the statistical analysis. X.X., S.L., and M.Y. provided

technical or material support. X.X., L.Y., Q.Z., and T.L. wrote the original draft. T.L. supervised the study. L.Y., Q.Z., and T.L. acquired the funding.

REFERENCES

1) EI-Serag HB, MD, M.P.H. Hepatocellular carcinoma. N Engl J Med 2011;365:18-27.
2) Kasper H-U, Drebber U, Stippel DL, Dienes HP, Gillessen A. Liver tumor infiltrating lymphocytes: comparison of hepatocellular and cholangiolar carcinoma. World J Gastroenterol 2009;15:5053.
3) **Sen DR**, **Kaminski J**, Barnitz RA, Kurachi M, Gerdemann U, Yates KB, et al. The epigenetic landscape of T cell exhaustion. Science 2016;354:1165-1169.
4) Chiossone L, Dumas PY, Vienne M, Vivier E. Natural killer cells and other innate lymphoid cells in cancer. Nat Rev Immunol 2018;18:671-688.
5) Vivier E, Artis D, Colonna M, Diefenbach A, Di Santo JP, Eberl G, et al. Innate lymphoid cells: 10 years on. Cell 2018;174:1054-1066.
6) **Sonnenberg GF**, **Hepworth MR**. Functional interactions between innate lymphoid cells and adaptive immunity. Nat Rev Immunol 2019;19:599-613.
7) Halim TYF. Group 2 innate lymphoid cells in disease. Int Immunol 2016;28:13-22.
8) Halim T, Steer C, Mathä L, Gold M, Martinez-Gonzalez I, McNagny K, et al. Group 2 innate lymphoid cells are critical for the initiation of adaptive T helper 2 cell-mediated allergic lung inflammation. Immunity 2014;40:425-435.
9) Salimi M, Barlow JL, Saunders SP, Xue L, Gutowska-Owsiak D, Wang X, et al. A role for IL-25 and IL-33-driven type-2 innate lymphoid cells in atopic dermatitis. J Exp Med 2013;210:2939-2950.
10) Liang Y, Yi P, Yuan DMK, Jie Z, Kwota Z, Soong L, et al. IL-33 induces immunosuppressive neutrophils via a type 2 innate lymphoid cell/IL-13/STAT6 axis and protects the liver against injury in LCMV infection-induced viral hepatitis. Cell Mol Immunol 2019;16:126-137.
11) Mchedlidze T, Waldner M, Zopf S, Walker J, Rankin A, Schuchmann M, et al. Interleukin-33-dependent innate lymphoid cells mediate hepatic fibrosis. Immunity 2013;39:357-371.
12) Silvestre-Roig C, Hidalgo A, Soehnlein O. Neutrophil heterogeneity: implications for homeostasis and pathogenesis. Blood 2016;127:2173-2181.
13) Zhang W, Wang H, Sun M, Deng X, Wu X, Ma Y, et al. CXCL5/CXCR2 axis in tumor microenvironment as potential diagnostic biomarker and therapeutic target. Cancer Commun 2020;40:69-80.
14) **Xu J**, **Guardado J**, Hoffman R, **Xu H**, Namas R, Vodovotz Y, et al. IL33-mediated ILC2 activation and neutrophil IL5 production in the lung response after severe trauma: a reverse translation study from a human cohort to a mouse trauma model. PLoS Med 2017;14:e1002365.
15) Wojno EDT, Artis D. Innate lymphoid cells: balancing immunity, inflammation, and tissue repair in the intestine. Cell Host Microbe 2012;12:445-457.
16) Wen L, Xin B, Wu P, Lin C-H, Peng C, Wang G, et al. An efficient combination immunotherapy for primary liver cancer by harmonized activation of innate and adaptive immunity in mice. Hepatology 2019;69:2518-2532.
17) Han G, Spitzer MH, Bendall SC, Fantl WJ, Nolan GP. Metal-isotope-tagged monoclonal antibodies for high-dimensional mass cytometry. Nat Protoc 2018;13:2121-2148.
18) Sanjana NE, Shalem O, Zhang F. Improved vectors and genome-wide libraries for CRISPR screening. Nat Methods 2014;11:783-784.
19) Simoni Y, Fehlings M, Kløverpris HN, McGovern N, Koo S-L, Loh CY, et al. Human innate lymphoid cell subsets possess tissue-type based heterogeneity in phenotype and frequency. Immunity 2017;46:148-161.
20) Hol J, Wilhelmsen L, Haraldsen G. The murine IL-8 homologues KC, MIP-2, and LIX are found in endothelial cytoplasmic granules but not in Weibel-Palade bodies. J Leukoc Biol 2010;87:501-508.
21) Bernink J, Krabbendam L, Germar K, de Jong E, Gronke K, Kofoed-Nielsen M, et al. Interleukin-12 and -23 control plasticity of CD127+ group 1 and group 3 innate lymphoid cells in the intestinal lamina propria. Immunity 2015;43:146-160.
22) **Zhang K**, **Xu X**, Pasha MA, Siebel CW, Costello A, Haczku A, et al. Cutting edge: notch signaling promotes the plasticity of group-2 innate lymphoid cells. J Immunol 2017;198:1798-1803.
23) **Gasteiger G**, **Fan X**, Dikiy S, Lee SY, Rudensky AY. Tissue residency of innate lymphoid cells in lymphoid and nonlymphoid organs. Science 2015;350:981-985.
24) Bie Q, Zhang P, Su Z, Zheng D, Ying X, Wu Y, et al. Polarization of ILC2s in peripheral blood might contribute to immunosuppressive microenvironment in patients with gastric cancer. J Immunol Res 2014;2014:923135.
25) Jovanovic IP, Pejnovic NN, Radosavljevic GD, Pantic JM, Milovanovic MZ, Arsenijevic NN, et al. Interleukin-33/ST2 axis promotes breast cancer growth and metastases by facilitating intratumoral accumulation of immunosuppressive and innate lymphoid cells. Int J Cancer 2014;134:1669-1682.
26) **Chevalier MF**, **Trabanelli S**, Racle J, Salomé B, Cesson V, Gharbi D, et al. ILC2-modulated T cell–to-MDSC balance is associated with bladder cancer recurrence. J Clin Invest 2017;127:2916-2929.
27) Jeffery HC, McDowell P, Lutz P, Wawman RE, Roberts S, Bagnall C, et al. Human intrahepatic ILC2 are IL-13positive amphiregulinpositive and their frequency correlates with model of end stage liver disease score. PLoS One 2017;12:e0188649.
28) Kim BS, Siracusa MC, Saenz SA, Noti M, Monticelli LA, Sonnenberg GF, et al. TSLP elicits IL-33-independent innate lymphoid cell responses to promote skin inflammation. Sci Transl Med 2013;5:170ra116.
29) Voehringer D, Koschella M, Pircher H. Lack of proliferative capacity of human effector and memory T cells expressing killer cell lectinlike receptor G1 (KLRG1). Blood 2002;100:3698-3702.
30) Henson SM, Franzese O, Macaulay R, Libri V, Azevedo RI, Kiani-Alikhan S, et al. KLRG1 signaling induces defective Akt (ser473) phosphorylation and proliferative dysfunction of highly differentiated CD8+ T cells. Blood 2009;113:6619-6628.
31) Huntington ND, Tabarias HY, Fairfax K, Brady J, Hayakawa Y, Degli-Esposti MA, et al. NK cell maturation and peripheral homeostasis is associated with KLRG1 up-regulation. J Immunol 2007;178:4764-4770.
32) **Li Q**, **Li D**, **Zhang X**, Wan Q, Zhang W, Zheng M, et al. E3 Ligase VHL promotes group 2 innate lymphoid cell maturation and function via glycolysis inhibition and induction of interleukin-33 receptor. Immunity 2018;48:e255.
33) Monticelli LA, Sonnenberg GF, Abt MC, Alenghat T, Ziegler CGK, Doering TA, et al. Innate lymphoid cells promote lung-tissue homeostasis after infection with influenza virus. Nat Immunol 2011;12:1045-1054.
34) **Kim J**, **Kim W**, Moon UJ, Kim HJ, Choi H-J, Sin J-I, et al. Intratumorally establishing type 2 innate lymphoid cells blocks tumor growth. J Immunol 2016;196:2410-2423.

35) **De Filippo K**, **Dudeck A**, Hasenberg M, Nye E, van Rooijen N, Hartmann K, et al. Mast cell and macrophage chemokines CXCL1/CXCL2 control the early stage of neutrophil recruitment during tissue inflammation. Blood 2013;121:4930-4937.
36) Baggiolini M, Walz A, Kunkel SL. Neutrophil-activating peptide-1/interleukin 8, a novel cytokine that activates neutrophils. J Clin Invest 1989;84:1045-1049.
37) Schwartz C, Khan AR, Floudas A, Saunders SP, Hams E, Rodewald H-R, et al. ILC2s regulate adaptive Th2 cell functions via PD-L1 checkpoint control. J Exp Med 2017;214: 2507-2521.
38) **Moral JA**, **Leung J**, **Rojas LA**, **Ruan J**, Zhao J, Sethna Z, et al. ILC2s amplify PD-1 blockade by activating tissue-specific cancer immunity. Nature 2020;579:130-135.

Author names in bold designate shared co-first authorship.

Supporting Information

Additional Supporting Information may be found at onlinelibrary.wiley.com/doi/10.1002/hep.31855/suppinfo.